

Evaporative attachment of slow electrons to alkali nanoclusters

Roman Rabinovitch, Chunlei Xia, and Vitaly V. Kresin

*Department of Physics and Astronomy,
University of Southern California, Los Angeles, California 90089-0484*

ABSTRACT

We have measured the abundance mass spectra of $\text{Na}^-_{n \sim 7-140}$ ions formed by low energy electron attachment to free nanoclusters. The distribution of anions is considerably restructured with respect to the neutral precursor beam. This restructuring can be understood quantitatively based on the evaporation cascade picture, whereby energy deposited by the captured electron is dissipated by the evaporative cooling of clusters. In addition, since the evaporation rates are sensitive to the cluster binding energies, the experimental data supplied an adjustment to the prior values of these quantities.

Low energy electron attachment to molecules and biomolecules has been extensively explored (see, e.g., the reviews [1-4] and references therein) because as an ionization technique it is quite different from electron bombardment or photoionization. Experimental work on electron attachment to clusters has focused primarily on fullerenes and molecular clusters (see, e.g., [1, 2, 5-9] and references therein).

Our group has studied binary collisions of slow electrons with free sodium nanoclusters in a beam [10-12]. Containing mobile delocalized electrons, alkali clusters are highly polarizable [13-15]. This leads to the appearance of strong long-range forces in interaction with charged particles [16] and to very high electron capture cross sections for $E_e < 1$ eV. Post-collision anions have been observed [12, 17], which raises new questions: how is the kinetic and binding energy of the captured electron dissipated; what are the relaxation channels; is there an effect on the cluster mass spectrum? For example, given that the beam of neutral clusters displays “magic numbers” at the electron-shell-closing sizes of $\text{Na}_{20,40,58,\dots}$ [13], will the daughter anions have abundance maxima at these same sizes – which have an enhanced population of neutral precursors – or will they be able to reorganize in accordance with the shell closing sequence of $\text{Na}_{19,39,57,\dots}^-$? It is also worth pointing out that the study of energy loss by electrons captured by free metal nanoclusters has clear parallels with research on the relaxation of carriers injected into size-quantized nanostructures and quantum dots [18].

In principle, for a free cluster the added electron energy can be accommodated by electron auto detachment, photon radiation, or cluster heating. To gain insight into the actual mechanism, we report on a detailed measurement and analysis of the formation of anion mass spectra by the attachment process. To our knowledge, this is the first such investigation over a wide cluster size range ($n \sim 7$ -140). We find that the mass spectrum does undergo extensive restructuring, which can be well explained by the statistical mechanism: the energy of the captured electron is promptly thermalized within the cluster, and the latter then cools by evaporating atom and dimer fragments.

An outline of the experiment is shown in Fig. 1. A supersonic-expansion source produced a collimated beam of neutral clusters. In the electron gun scattering region they were intersected

at a right angle by a beam of low energy electrons. The electrons were produced by a planar dispenser cathode (Spectra-Mat) and constrained into a ribbon-shaped beam by a set of grids, masks, and a collinear 400-gauss magnetic field [10, 19, 20]. Cluster anions born in the interaction region were extracted with ion optics, focused into a quadrupole mass filter (Extrel QPS9000), and detected by a channeltron electron multiplier (DeTech) equipped with a custom-made conversion dynode held at 16 kV. High voltage operation was necessary in order to efficiently detect the heavy negative ions.

Despite the effort devoted in the setup to the creation and detection of negative ions, the reality is that low-energy sources produce only a limited amount of electron flux. As a result, only $\sim 1\%$ of the original beam became negatively charged [10], and the remainder passed undisturbed into the end part of the apparatus, where it was ionized by focused UV light and mass analyzed by a second quadrupole [21]. The benefit of this arrangement is that it recorded both the anion (daughter) and the neutral (precursor) cluster mass spectra simultaneously, making it possible to follow and analyze their transformations without distortions due to beam variations.

The biggest experimental challenge lay in the aforementioned low ion yield. The typical mass-selected anion signal was below ten counts per second. To raise the beam intensity, we used high source temperatures and carrier gas pressures. The settings of the electron gun were optimized for maximum anion signal. The electron energy distribution was measured using the retarding potential technique [20], and the effective average energy of the electrons was found to be $E_e = 0.2$ eV [22]. The corresponding Langevin [23] electron capture cross sections for Na_{20} , Na_{40} , and Na_{58} are $\sigma_L \approx 1000 \text{ \AA}^2$, 1500 \AA^2 , and 1800 \AA^2 , respectively.

The measured anion mass spectra are shown in Fig. 2(a), displaying well-resolved mass peaks over a wide range. The distribution is significantly restructured relative to that of the neutral clusters, shown for comparison in Fig. 2(b). First, the overall envelope is moved to higher masses. Second, the magic numbers are lowered by one. Third, the relative intensities of the anion peaks between the magic numbers are in an inverse correlation with the intensities of the corresponding neutrals, which is not a simple pattern shift by one electron number. While the envelope change can be due to different detection efficiencies of the anions and of the precursor

cluster beam, and the magic number shift is intuitively attributable to the extra acquired electron, understanding the more subtle variations requires an accurate treatment.

The anions are unlikely to be in a metastable surface-bound electron state, because they are detected long ($\sim 10^{-5}$ s) after formation, and are too “floppy” and hot (see below) to sustain such a state. Radiative decay, if any, may become important only at collision energies above several eV, i.e., above the collective resonance frequencies [24]. Consequently, all the energy delivered by the captured electron (i.e., its initial kinetic energy E_{e^-} plus the cluster electron affinity EA) will promptly dissipate into the internal thermal energy of the cluster. If the amount of this energy is sufficient, prompt cluster evaporation will follow. We found that the data can indeed be elucidated on the basis of the “evaporative attachment” [25] picture. That is, anion formation is viewed as consisting of three steps.

(I) An electron is captured by the long-range polarization potential of the cluster. The cross section for this process has been found [10, 12] to be governed by the aforementioned Langevin formula, $\sigma_L = \left(2\pi^2 e^2 \alpha / E_{e^-}\right)^{1/2}$, where α is the electric polarizability of the cluster. This is a relatively smooth function of cluster size [15], hence the initial capture step will not spawn strong size-to-size intensity alterations.

(II) The energy supplied by the electron is promptly dissipated, heating up the cluster. The vibrational temperature (the term is employed as a measure of the internal energy contents) increases by $\Delta T = (E_{e^-} + EA) / C$, where the heat capacity of an n -atom cluster may be approximated by $C = (3n - 6)k_B$.

(III) The clusters cool [26, 27] by evaporating one or more atoms or dimers and losing internal energy with every step. The energy loss is $\Delta E = D_n^- + 2k_B T$, where D_n^- is the anion dissociation energy, the second term is the kinetic energy of the outgoing fragment, and T is the cluster temperature prior to evaporation [28]. This proceeds until the temperature drops so much that the evaporation rate becomes negligible on the experimental time scale, and the cluster size distribution at that point should then correspond to the recorded mass spectrum.

The evaporation rate can be expressed as [27, 29]

$$r(T) = \tau_0^{-1} n^{2/3} \exp(-D_n^- / k_B T^*), \quad (1)$$

where $T^* = T - D_n^- / 2C$, the second term reflecting the so-called finite-size correction [27].

Below, the factor τ_0 is chosen to be $\approx 10^{-12}$ s for consistency with the value used in Ref. [30] to deduce cluster dissociation energies (for a precise discussion of τ_0 see Ref. [27]). Eq. (1) makes it clear that the rate will be exponentially sensitive to the anion's dissociation energy and vibrational temperature (and thereby to the electron affinity). These quantities do oscillate from one cluster to the next, and the corresponding variations in the evaporative chain are, in point of fact, at the root of the observed restructuring of the anion abundance spectrum. Conversely, we see that in interpreting electron capture and transfer reactions it is essential to account for the accompanying fragmentation effects [31].

The capture of an electron affects the evaporation process in two ways. First, it changes the dissociation energy by altering the number of delocalized electrons in the cluster, i.e., by modifying the electronic shell levels and their occupation. Second, the energy deposited by the electron heats up the cluster and engenders a jump in the evaporation rate. By using Eq. (1) and including both of these factors, the post-attachment evaporation rates for anions can be calculated. The required ingredients are: the internal temperatures of the original neutral clusters, their electron affinities, and the anions' monomer and dimer fragmentation energies and branching ratios.

Applying the analogue of Eq. (1) to the original neutral beam, one can define the temperature T_n for each Na_n cluster based on its lifetime τ (i.e., the flight time from the source) and on D_n . This approach is described in detail in Ref. [27], and has been found to be in good agreement with experimental data [28, 33]. Its result is that T_n may be taken as a flat distribution $F(T)$ spread between T_n^{\min} and T_n^{\max} with

$$T_n^{\max} = D_n / k_B \ln(n^{2/3} \tau / \tau_0) + D_n / 2C, \quad T_n^{\min} = T_{n+1}^{\max} - D_{n+1} / C. \quad (2)$$

The initial temperature of the corresponding anion, T_n^- , is found by adding the amount ΔT specified above, with EA from the Na_n^- photoelectron spectra [34, 35]. Typical post-

attachment anion temperatures and temperature spreads range from 520 K and 50K for Na_{40} , to 1000 K and 480K for Na_6 .

So the probability for a newly formed anion to evaporate by the time t is, in view of the flatness of $F(T)$,

$$P_n = \int_{T_{n,\min}^-}^{T_{n,\max}^-} (1 - e^{-r(T)t}) dT, \quad (3)$$

Finally, we need the anion dissociation energies D_n^- . Unfortunately, experimentally only cation data, D_n^+ , are available [30], and for negative ions theoretical values have been computed only for Na_n^{2-} [36]. Using the droplet model [37], the total energies of neutral and ionic clusters can be related as follows:

$$E_n = E_n^+ + \left(W - \frac{5}{8}e^2/R_n\right), \quad E_n^- = E_n - \left(W - \frac{3}{8}e^2/R_n\right), \quad (4)$$

(W is the work function, $R_n = r_{\text{Wigner-Seitz}} n^{1/3}$ is the cluster radius). It is straightforward to show that shell corrections do not affect these expressions as long as the number of valence electrons remains unchanged. (Jellium model calculations recover the same result [36].) The dissociation energies of neutral and anion clusters can be deduced from these formulae by subtraction and expansion to first order in $1/n$:

$$D_n \approx D_{n+1}^+ - \frac{5}{24} \left(e^2/R_n\right) n^{-1}, \quad D_n^- \approx D_{n+1}^- + \frac{1}{8} \left(e^2/R_n\right) n^{-1}. \quad (5)$$

Cation dissociations energies were originally determined [30] by using RRK unimolecular reaction theory which contained uncertainties in the state-density and frequency factors. The fact that the electron capture experiment is sensitive to cluster binding energies allowed us to correct these values: we found that in order to reproduce the data it was necessary to adjust the evaporation energies of Ref. [30] downward by 25% for Na_{9-19}^+ and by 15% for Na_{20-36}^+ .

Modeling the anion abundance spectra begins with the measured mass spectrum of the neutral precursors, which is convoluted with σ_L to generate the parent anion population. Next, evaporative cooling chains are calculated for every cluster. It is important to incorporate both

atom and dimer loss pathways [30, 38]. The resulting distribution is weighted by an instrumental factor \sqrt{n} (the probability for an anion to exit the electron collision region [20]), and may now be compared with the experimental anion mass spectrum.

This comparison is shown in Fig. 3 for clusters up to Na_{33}^- (the largest size for which dissociation cascades can be fully deduced from the dissociation energy data [30]). The calculation matches the experimental pattern very well, including such nontrivial features as the aforementioned intensity variations of open-shell clusters, and the unusual feature that the Na_{18}^- peak is stronger than the closed-shell Na_{19}^- (this is due to extensive evaporation of the parent Na_{20}^-).

Thus generation of negative cluster ions by low-energy electron attachment is accurately described by the presented framework: efficient capture by long-range forces, followed by thermalization and by significant rearrangement of the abundance distribution by evaporative emission of atom and dimer fragments. Since this evaporative cooling is exponentially sensitive to cluster temperatures and dissociation energies, slow-electron capture offers a useful window into the statistical and binding properties of metal clusters.

Evaporative attachment will be important until nanoclusters grow to be too massive to heat up appreciably. An estimate shows that evaporation becomes negligible for $\text{Na}_{n \gtrsim 10^3}$, at which point the anion mass spectrum should mirror that of the neutral precursor beam.

We are grateful to Dr. K. Hansen and Dr. R. Moro for very helpful discussions, to D. Boettger for experimental help, and to J. Ray and DeTech for constructing the high-voltage channeltron. This research was supported by NSF.

Fig. 1. Outline of the experiment. A neutral Na cluster beam was created by supersonic expansion through a 75 μm nozzle. The source body was kept at 660 $^{\circ}\text{C}$ and the Ar carrier gas pressure varied from 300 kPa to 600 kPa. Inside the electron gun the cluster beam ($1.4\text{ mm} \times 1.4\text{ mm}$ in cross section) was intersected by a ribbon of slow electrons ($1.4\text{ mm} \times 25.4\text{ mm}$, $\sim 10\text{ }\mu\text{A}$ current). The negatively charged products were extracted with an electrostatic lens, filtered by a quadrupole mass analyzer (QMA), and detected by a channeltron. The remaining neutral clusters passed into the next chamber, where they were ionized by a UV lamp and detected by another QMA. The abundance spectra of precursor and anion clusters were recorded simultaneously.

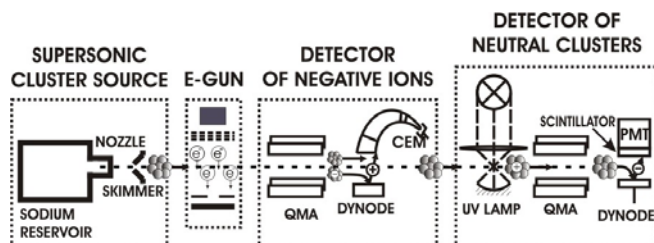


Fig. 2. Mass spectra of the electron attachment products (a) and the precursor beam (b). The anion pattern differs from that of the neutral precursors: the magic numbers are shifted and the relative abundances of open-shell clusters are altered. Colors in (a) represent spectra taken under different conditions: for each segment the cluster source was optimized for maximum precursor intensity, and the settings of the first QMA were adjusted to achieve the strongest mass-resolved anion signal.

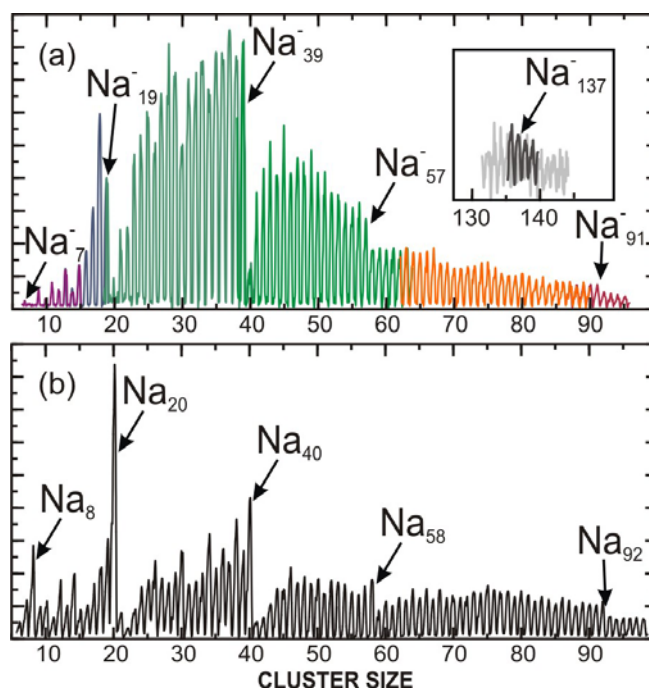
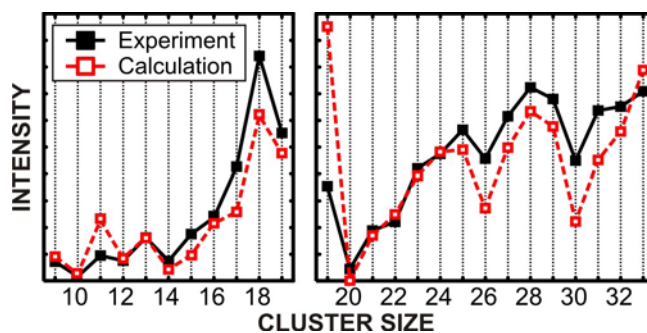


Fig. 3. A comparison of the measured and calculated relative abundance distributions of Na_n^- clusters formed by low-energy electron attachment. The two panels correspond to data segments acquired under different optimization conditions. As described in the text, energy released by the captured electron is rapidly thermalized within the cluster, and the resulting cooling via evaporation of atoms and dimers restructures the abundance spectrum. The modeled distribution was derived by convoluting the evaporation pathways with the mass spectrum of the precursor neutral beam. (The split of the Na_{19}^- values in the right-hand panel is an artifact of QMA discrimination against low masses for this data segment.)



REFERENCES

- [1] E. Illenberger, in *Photoionizaion and Photodetachment*, ed. by C.-Y. Ng (World, Singapore, 2000).
- [2] H. Hotop *et al.*, Adv. Atom. Mol. Opt. Phys. **49**, 85 (2003).
- [3] L. Sanche, Eur. Phys. J. D. **35**, 367 (2005).
- [4] J.-P. Schermann, *Spectroscopy and Modeling of Biomolecular Building Blocks* (Elsevier, Amsterdam, 2007).
- [5] O. Ingolfsson and A. M. Wodtke, J. Chem. Phys. **117**, 3721 (2002).
- [6] M. Lezius, Int. J. of Mass Spectrom. **223**, 447 (2003).
- [7] M. Farnik and J. P. Toennies, J. Chem. Phys. **118**, 4176 (2003).
- [8] A. A. Vostrikov and D. Y. Dubov, Tech. Phys. **51**, 1537 (2006).
- [9] S. Denifl *et al.*, Phys. Rev. Lett. **97**, 043201 (2006).
- [10] V. Kasperovich *et al.*, Phys. Rev. A **60**, 3071 (1999).
- [11] V. Kasperovich *et al.*, Phys. Rev. Lett. **85**, 2729 (2000).
- [12] V. Kasperovich *et al.*, Phys. Rev. A **62** 063201 (2000).
- [13] W. A. de Heer, Rev. Mod. Phys. **65**, 611 (1993).
- [14] M. Broyer *et al.*, C. R. Physique **3**, 301 (2002).
- [15] G. Tikhonov *et al.*, Phys. Rev. A **64** 063202 (2001).
- [16] V. V. Kresin and C. Guet, Philos. Mag. B **79**, 1401 (1999).
- [17] Ş. Şenturk *et al.*, J. Phys. B **33**, 2763 (2000).
- [18] J. Urayama *et al.*, Phys. Rev. Lett. **86**, 4930 (2001).
- [19] R. E. Collins *et al.*, Rev. Sci. Instrum. **41**, 1403 (1970).
- [20] V. G. Kasperovich, Ph. D. thesis, University of Southern California, 2001.
- [21] Many measurements of size-dependent properties of alkali clusters have shown that mass spectra produced by filtered near-threshold UV ionization closely reflect the population of the original neutral beam [13].

- [22] The average energy was calculated by convoluting the electron distribution with the attachment cross section σ_L .
- [23] E. W. McDaniel, *Atomic Collisions: Electron and Photon Projectiles* (Wiley, New York, 1989).
- [24] L. G. Gerchikov, A. N. Ipatov, and A. V. Solov'yov, *J. Phys. B* **31**, 2331 (1998).
- [25] J. M. Weber *et al.*, *Eur. Phys. J. D.* **7**, 587 (1999).
- [26] C. E. Klots, *J. Chem. Phys.* **83**, 5854 (1985).
- [27] K. Hansen and U. Näher, *Phys. Rev. A* **60**, 1240 (1999).
- [28] P. Brockhaus *et al.*, *Phys. Rev. A* **59**, 495 (1999).
- [29] F. Lépine and C. Bordas, *Phys. Rev. A* **69**, 053201 (2004).
- [30] C. Bréchignac *et al.*, *J. Chem. Phys.* **90**, 1492 (1989).
- [31] For example, in an experiment on electron transfer from Kr^{**} atoms to K_n clusters [32], the distribution of K_{3-26}^- was similar to the one reported here. The authors postulated that the pattern was due to strong cluster-shape related variations in the attachment cross section, and neglected post-transfer evaporation effects. We find, however, that the long-range cross sections are relatively smooth functions of size, and mass spectrum restructuring is in reality due to evaporation cascades.
- [32] M. Nagamine, K. Someda, and T. Kondow, *Chem. Phys. Lett.* **229**, 8 (1994).
- [33] P. Dugourd *et al.*, *Chem. Phys.* **218**, 163 (1997).
- [34] M. Moseler *et al.*, *Phys. Rev. B* **68**, 165413 (2003).
- [35] O. Kostko *et al.*, *Eur. Phys. J. D.* **34**, 133 (2005).
- [36] C. Yannouleas and U. Landman, *Phys. Rev. B* **48**, 8376 (1993).
- [37] M. P. J. van Staveren *et al.*, *Phys. Rev. B* **35**, 7749 (1987).
- [38] C. Bréchignac *et al.*, *J. Chem. Phys.* **93**, 7449 (1990).